Instrumentation of coherent X-ray imaging and the primary experimental results*

XU Rui(许锐)[1)] LIU Chao-Pei(刘超培)

Institute of High Energy Physics, CAS, Beijing 100049, China

Abstract Coherent X-ray microscopy has advanced towards higher-energy, more brilliant sources over the past decade since its demonstrations, and many advancements have been made towards optimizing this imaging technique. Here we present both the experimental instrument for obtaining diffraction patterns and the primary reconstruction of yeast cell 2D projection. In addition, the characteristics of the existing optics at BL29XUL of SPring-8 Facility and the method of image reconstruction are discussed.

Key words CXDM, oversampling, image reconstruction, phase retrieval

PACS 87.59.-e

1 Introduction

Coherent X-ray diffraction microscopy (CXDM) is a progressive imaging technique whereby iterative algorithms replace lenses and aberration-free, diffraction-limited images may be obtained. Such images are obtained by measuring the diffracted intensities in the far-field, where the lost phase information is embedded. To date, many nano-structures of amorphous samples have been revealed by CXDM including cell, virus, nano-porous materials and so on.

The initial realization that an oversampled diffraction pattern could be inverted to the scattering structure was first pointed out by Sayre (1952) [1] in conjunction with the phase problem of crystallography. However, it was not proved until 1999 that Miao et al. [2] demonstrated the first experimental image. This X-ray imaging technique has several key advantages. In the first place, high energy photons are notoriously difficult to focus, and optics-based imaging systems that rely upon such components achieve resolutions limited by the fabrication precision of the optics which is several orders larger than the wavelength. However, by using CXDM, there is no such a resolution limitation, and in principle, diffraction-limited images may be obtained. Additionally, whereas electron-based microscopes can obtain high resolution, they are also limited by stringent constraints upon sample thickness. CXDM has no such limitations, and in principle, sub-10 nm resolution images can be obtained from several-micron thick samples such as the whole unstained cells.

When those noncrystalline samlples are illuminated by a coherent, monochromatic beam, the far-field diffraction pattern is continuous. The continuous pattern can be sampled at an arbitrary frequency. When the sample frequency is two times finer than the Nyquist interval, the number of independent intensity points is more than the number of unknown variables. So the missing phase is actually encoded in the oversampled pattern and the lost phase can be retrieved directly using an iterative algorithm [3]. These algorithms are often based on the iterative hybrid input–output method introduced in the 1980s by Fienup (1982) [4].

2 Experimental set-up

Large synchrotron facilities offer superior beam quality, where small beam divergence, continuous tunable energy, and high beam flux facilitate the gain of high resolution data. The layout of the synchrotron facility is centered around the main storage ring and branched with multiple beamlines which are tangent to the ring. BL29XUL is a coherent X-ray beamline built at the Super Photon Ring 8 GeV (SPring-

Received 5 March 2009, Revised 28 April 2009

* Supported by 973 Program of the Ministry of Science and Technology (2009CB918600)

1) E-mail: xur@ihep.ac.cn

8) Synchrotron [5]. It consists of three major parts: the front-end, the optics hutch and the experimental hutch. One SPring-8 standard in vacuum undulator insertion device (ID) is located at the front-end, a SPring-8 standard double crystal monochromator (DCM) and a pair of reflecting mirrors are located in the optics hutch. The Coherent X-ray Diffraction Microscopy (CXDM) setup is installed in the experimental hutch1 (EH1) which is 52 m away from the source [5].

As is shown in Fig. 1, the CXDM set-up includes 7 main components which are i) pinhole; ii) two corners; iii) photodiode; iv) beam attenuator; v) sample stage; vi) beam stop; and vii) CCD detector.

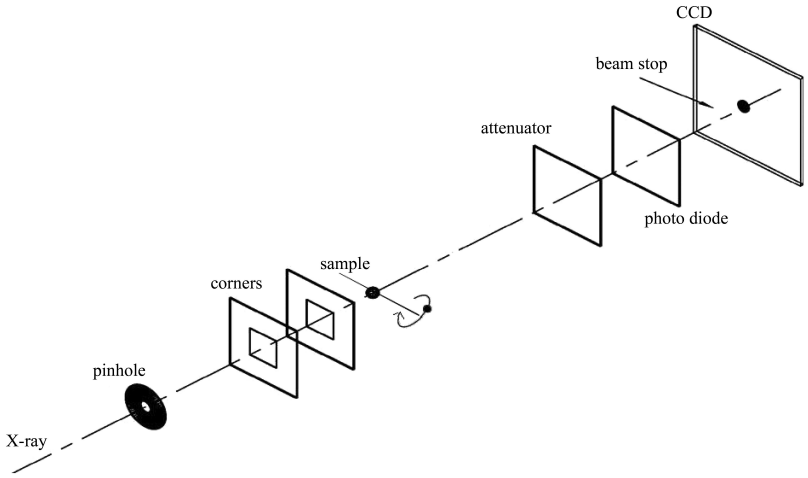

Fig. 1. Schematic layout of the instrument.

The size of the beam delivered into EH1 is 0.7 (V) mm × 1.3 (H) mm. To limit the size of the beam, a 20um-sized pinhole aperture is installed about 1 m upstream from the sample. Downstream from the pinhole, the bottom-right corners of two silicon nitride frames are used as L-shaped slits to minimize the scattering from the pinhole edges. The combination of pinhole and corners can produce clean diffraction signal in three adjacent quadrants. Correspondingly, in front of the CCD detector, a beam stop is used to block both the direct beam and the noisy quadrant. However, the diffraction pattern in missing quadrant can be recovered by using centrosymmetric operation, which is due to the fact that the scattering density of the sample is usually real in hard X-ray region. To avoid CCD's damage caused by saturation exposure, an attenuator is mounted in front of the beam stop if the experiment operator tries to find the direct beam position on CCD chip. Between the beam stop and the attenuator, a photodiode is necessary to monitor the beam status constantly when the components before photodiode are being tuned and aligned by user. In sample chamber, the motor-driving sample stage has three directions including vertical movement, horizontal movement and rotation for both 2D and 3D diffraction microscopy.

Figure 2 below is the photocopy of our set-up, all the motored components which can be controlled by the Labview software suite, are connected with an operating computer through interface card.

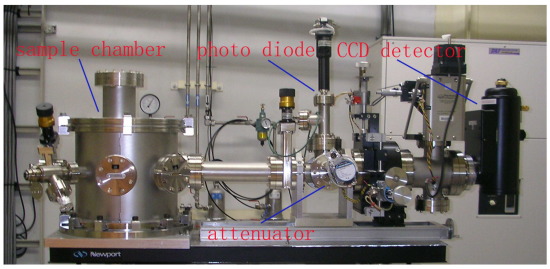

Fig. 2. The photocopy of the instrument.

3 Image reconstruction

We have an a priori knowledge that the sample is noncrystalline finite object, so $\rho(x,y)$ is a density distribution which includes the density region and the surrounding non-density region. To characterize how Fourier transform equations are overdetermined, a concept called the oversampling ratio σ was introduced to define the oversampling degree (1),

$$\sigma = \frac{S_1 + S_2}{S_1}. \tag{1}$$

Here, S_1 is the area of the sample, S_2 is the area of the sample's surrounding region.

An oversampled diffraction pattern with $\sigma > 2$ encodes the phase in the diffraction intensity [6]. To retrieve the embedded phase, an efficient approach is applying optimization methods: error reduction [7], hybrid input-output [7], difference map [8], shrink-wrap [9], guided hybrid input-output [10], modified hybrid input-output [11], all of which iterate between real and reciprocal space. Here, we introduce the hybrid input-output (HIO) algorithm which has global optimization characteristics. The procedure is as follows:

1) Use a set of random phase as initial phase, and we set the blocked central diffraction signal to 0.

2) Obtain a reconstructed image $\rho'_j(x,y)$ by using inverse Fourier transform.

3) Apply the image constraints to obtain the updated image $\rho_j(x,y)$ as follows:

$$\rho_j = \begin{cases} \rho'_j(x,y) \\ \quad \text{if } (x,y) \in S_1 \text{ and } \rho'_j(x,y) \geqslant 0 \\ \rho_{j-1}(x,y) - \beta\rho'_j(x,y) \\ \quad \text{if } (x,y) \notin S_1 \text{ or } \rho'_j(x,y) < 0 \end{cases}. \quad (2)$$

Here, β is a constant to adjust the convergence process which was set to 0.9. S_1 is the density region.

4) Obtain the updated phase and the updated central diffraction signal by using Fourier transform. Then we iterate Step 2) – 4).

In practice, the detector integrates the scattered photons within specific solid angles, which is determined by

$$I_{\rm M} = I_{\rm S} \otimes \Delta, \quad (3)$$

where $I_{\rm M}$is the measured diffraction pattern, $I_{\rm S}$ is the exactly sampled diffraction intensity, Δ is the rectangular function determined by the size of the detector's pixel, and $\otimes$ is convolution operator. So it's possible to exactly sample diffraction intensity through deconvolution operation before image reconstruction gets started [12].

$$I_{\rm S} = FT\left\{\frac{FT^{-1}[I_{\rm M}]}{FT^{-1}[\Delta]}\right\} = FT\left\{\frac{FT^{-1}[I_{\rm M}]}{{\rm sinc}(x)}\right\}. \quad (4)$$

With the instrument described above, we have recorded the diffraction patterns from a noncrystalline sample by using coherent X-rays with a wavelength of 2.48 Å. Then we apply the HIO algorithm to retrieve the missing phase and reconstruct the real-space image as follows:

Figure 3 shows the diffraction pattern of a single, unstained yeast cell and the characteristic structures of the diffraction pattern reflecting the general round shape of the yeast cell. The size of the yeast cell is ~1.6 um, and the high-density region is the cell nucleolus.

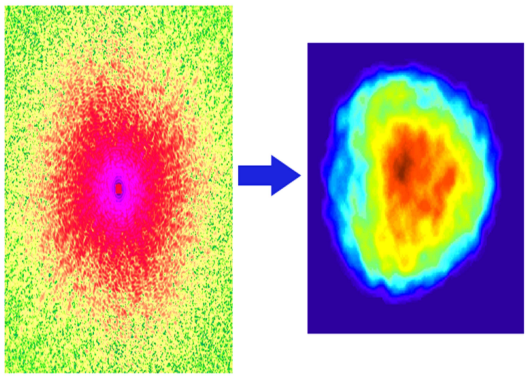

Fig. 3. X-ray diffraction pattern obtained from a single, unstained yeast cell. High-contrast image reconstructed from the pattern where the background and the surroundings of the yeast cell were completely removed.

4 Conclusion

The coherent X-ray diffraction imaging method and the set-up at BL29XUL of Spring 8 synchrotron radiation facility have been described, for which the costs of the camera and the installation are minimal. The experimental performance of the coherent X-ray optics has been demonstrated. Fine structure of the yeast cell was successfully observed using high-coherence X-rays. Contrast and resolution were improved incredibly using high-coherence X-rays.

References

1 Sayre D. Acta Crystallogr., 1952, **5**: 843
2 MIAO J, Charalambous P, Kirz J, Sayre D. Nature (London), 1999, **400**: 342
3 MIAO J, Ishikawa T, Earnest T, SHEN Qun. Annu. Rev. Phys. Chem., 2008, **59**: 387–409
4 Fienup J R. Appl. Opt., 1982, **21**: 2758
5 Tamasakua K, Tanaka Y et al. Nucl. Instrum. Methods A, 2001, **467-468**: 686–689
6 MIAO J, Ishikawa T, Anderson E H, Hodgson K O. Phys. Rev. B, 2003, **67**: 174104
7 Fienup J R. Opt. Lett., 1978, **3**: 27–29
8 Elser V. J. Opt. Soc. Am. A, 2003, **20**: 40–55
9 Marchesini S. Rev. Sci. Instrum., 2007, **78**: 011301
10 CHEN C C, MIAO J, WANG C W, Lee T K. Phys. Rev. B, 2007, **76**: 064113
11 Nishino Y. Phys. Rev. B, 2003, **68**: 220101
12 SONG Chang-Yong, Ramunno-Johnson D. Phys. Rev. B, 2007, **75**: 012102